Stretch-twist-fold and *ABC* nonlinear dynamos: Restricted chaos

Samuel I. Vainshtein,[1] Roald Z. Sagdeev,[2] and Robert Rosner[1]
[1]*Department of Astronomy and Astrophysics, University of Chicago, Illinois 60637*
[2]*East West Space Science Center, University of Maryland, College Park, Maryland 20742-3280*
(Received 27 February 1997)

We present direct numerical simulations for nonlinear dynamos, based on a Lagrangian approach that allows us to compute for relatively high effective magnetic Reynolds numbers, $R_m \sim (1\text{–}3)\times 10^4$. The particular systems we study and contrast are the stretch-twist-fold (STF) and the *ABC* flow dynamos. In the case of the STF dynamo, we show that whereas small-scale magnetic fluctuations are suppressed in the nonlinear regime, they still remain sufficiently large so that the STF dynamo still cannot be considered (in this nonlinear regime) a paradigm for a fast dynamo. Our numerical study of the *ABC* flow dynamo indicates, first, that during the period of kinematic behavior, there is no growth of a large-scale magnetic field, and that any large-scale field components are subject to classical turbulent diffusion; second, we show that if back reactions (due to magnetic tension) are taken into account this diffusion is highly restricted. We refer to this behavior as ''restricted chaos.'' [S1063-651X(97)10508-6]

PACS number(s): 05.45.+b, 52.30.−q, 47.52.+j, 47.53.+n

I. INTRODUCTION

The ''fast'' generation of magnetic fields remains an unsolved problem, even in the linear approximation. In the latter limit, corresponding to the ''kinematic'' dynamo problem (for which the velocity field is presumed to be given), this ''dynamo problem'' reduces to finding flow that lead to exponentially growing solutions for the magnetic field. This problem has turned out to be remarkably difficult: it is known that it cannot be reduced to two dimensions because one can show that no dynamo is possible in this limit [1]; similarly, symmetric dynamos are also impossible [2]. Indeed, there are no known general solutions for the simplest kinematic problem; and simple physical arguments are confounded by the fact that the geometric and topological structure of the magnetic field quickly becomes very complicated as dynamo action proceeds. This seemingly intrinsic complexity of dynamo-generated magnetic fields appears to be characteristic of virtually all numerical simulation (cf. [3,4]). A further fundamental difficulty arises because the eigenfunctions of the induction equation operator are characterized by a diffusive scale δ, rather than by the typical scale of the velocity field l [5]. The scale δ turns out to be typically very small when compared to the flow scale length l: a rough estimate gives $\delta = l/R_m^{1/2}$, where R_m is the magnetic Reynolds number ($\equiv vl/\eta$, with v atypical velocity and η the magnetic diffusivity); as the magnetic Reynolds number is generally very large in most cases of interest, the scale δ becomes very small. This difficulty also arises in numerical calculations, in which one attempts to compute with as large a magnetic Reynolds number as possible; as a result, there is an enormous disparity between the smallest diffusive structures and the spatial scales characterizing (for example) the energy-containing eddies in the flow. This scale separation problem is a by now classic stumbling block for treating dynamo action accurately and realistically.

One possibility for avoiding this problem is to solve the ideal case, $\eta = 0$ (corresponding to the limit $R_m \to \infty$), by using the Cauchy solution [3,4]. Since ''fast dynamo'' action is generally interpreted to mean that the growth rate of the magnetic field becomes independent of the diffusivity η in this limit [6], one might therefore hope that fast dynamo action could be found for $\eta = 0$. More specifically, in spite of the strong likelihood of growing small-scale magnetic fluctuations, one might nevertheless expect that appropriate flows would also generate large-scale magnetic flux, which in turn would not be affected by a small diffusivity; such flux growth at large scales would suggest the existence of a fast dynamo for the large-scale field component.

However, it has long been thought [6] that a finite, though small, diffusivity is crucial for the operation of fast dynamos. Indeed, the notion of fast dynamos originated as an analog to fast processes in fluid turbulence; for example, turbulent diffusion (of, say, a scalar passive field) is a fast process; i.e., the turbulent diffusion coefficient is independent of the molecular diffusivity. This happens because there exists an energy cascade to small scales, where diffusion acts, and thus destroys inhomogeneities of scalar fields. It is usually presumed that fast dynamos work in the same way, i.e., that the scale of the magnetic field must be reduced to diffusive scales by the flow before generation can start to work, provided generation is more efficient than diffusion. Thus, roughly speaking, a dynamo creates new field lines, and one would think that this can be done only on diffusive scales. This point of view explains why the eigenfunctions of the induction equation operator are characterized by diffusive scales [5]. Presumably, laminar dynamos work analogously, that is, the field adjusts itself to (small-scale) eigenfunctions after scale reduction, and only then the dynamo starts to operate [7,8].

A different perspective on this issue is obtained by considering the role of turbulent diffusion in fast (turbulent) dynamos (cf. Parker [9]). Consider, for example, the case of cyclic magnetic fields, as are encountered in studies of the solar cycle. In that case, turbulent diffusion is required in order to ''get rid'' of old magnetic flux from former cycles.

There is no universal agreement as to which of these two approaches (i.e., either the flux is generated on large scales, essentially independently of the diffusivity, or this generation is actually produced on diffusive scales) is correct. It may be that both are correct, that is, that both of these processes operate in naturally occurring dynamos. One of the cornerstones of the first approach is the stretch-twist-fold (STF) motion [6,10]. Indeed, the STF seems to generate magnetic flux without invoking diffusivity. Amazingly enough, this picture—which played such an important role in the development of dynamo theory (cf. [3])—was based just on a simple illustration, that is, on a sketch of this process. Recent numerical simulations of the STF flow [11] showed, however, that the STF flow actually leads to very complicated fields; in other words, the STF flow is from this perspective not special, but rather leads to the kind of field behavior that other complex (turbulent) flows also produce. This result is true at least for the case in which the STF is represented by a continuous, and therefore realistic, velocity. (If one allows for discontinuous flows, then there is no need to appeal to the STF as there are much simpler flows that result in fast dynamo action [3].)

The question of whether or not there are strong magnetic fluctuations during dynamo action is a matter of pure semantics if the discussion is restricted only to the kinematic regime. In this regime, all that matters is if the large-scale field B_0 grows rapidly; small-scale fields could then be smoothed out by finite diffusivity, or by nonlinear effects not accounted for in the kinematic regime. However, in the nonlinear regime the situation is quite different. In this case, field growth might stop when the small-scale fields reach equipartition with the kinetic energy. Therefore, the ratio $\langle B^2\rangle/\langle B_0^2\rangle$ may play an important role in the dynamics. It has been suggested [7] that this ratio scales as

$$\frac{\langle B^2\rangle}{\langle B_0^2\rangle}\sim R_m^n, \tag{1}$$

with an exponent n not small compared to unity. This conjecture is supported by various calculations, including direct numerical simulations [12]. In particular, it became apparent that in the two-dimensional case, turbulent diffusion is strongly suppressed by a weak large-scale magnetic field. In three dimensions, the so-called alpha effect—the generation of large-scale field—is suppressed in a very similar manner [13]. These direct numerical simulations are restricted to quite modest values of the magnetic Reynolds number (typically, in the range 10^2-10^3) because of their extraordinary computational demands. One of the goals of this paper is to study the processes of turbulent diffusion and turbulent generation in the limit of $R_m\to\infty$, and in the fully developed nonlinear regime; this requires a different computational strategy than reliance upon direct numerical simulation of the Navier-Stokes and induction equations, namely, one based upon use of the Cauchy solution (as developed by us in an earlier paper on the linear growth of the STF [11]).

The main focus of this paper is therefore the nonlinear STF flow. As shown previously [11], the STF results in rather complicated, indeed chaotic, behavior of the field lines, instead of the highly symmetric field geometry originally expected. As a result, one finds that the level of magnetic field fluctuations is high, that is, the ratio $\langle B^2\rangle/\langle B_0^2\rangle$ in Eq. (1) is large. One might expect that the Lorentz force would tend to smooth out the fluctuations, thus diminishing them; in fact, the numerator $\langle B^2\rangle$ is restricted in the nonlinear limit by the backreaction of the magnetic field, and therefore one might expect the critical parameter n to decrease when compared to what one obtains in the kinematic STF limit. Simulations reveal, however, a more complicated picture, so that this simple expectation is realized only in part.

Our paper is organized as follows: Sec. II develops the basic formulation of the STF problem, Sec. III gives a brief overview of the kinematic limit, and Sec. IV treats the basic results of nonlinear calculations. We focus on the special case of ABC flows in Sec. V, discuss the effects on turbulent diffusion in Sec. VI, and summarize our results, and present our conclusions, in Sec. VII.

II. FORMULATION OF THE PROBLEM

In the linear limit, the dynamo problem reduces to looking for (exponentially) growing solutions of the induction equation

$$\frac{\partial \mathbf{B}}{\partial t}=\nabla\times[\mathbf{v}\times\mathbf{B}]+\eta\nabla^2\mathbf{B}. \tag{2}$$

In the kinematic approach, the velocity field $\mathbf{v}$ is given, so that no dynamics is involved. In this paper, the velocity is given not directly, but as a solution of the Newton law,

$$\frac{d\mathbf{v}}{dt}=\mathbf{F}+\mathbf{D}, \tag{3}$$

where $\mathbf{F}$ is a (time-dependent) forcing and $\mathbf{D}$ represents damping. The external forcing function $\mathbf{F}$ is such as to generate the desired velocity field; the details of specifying the forcing function $\mathbf{F}$ for the STF are given in the Appendix, and for ABC flow are described in Sec. V. The damping is required in order to eliminate the possibility of unbounded flow velocities in the absence of any other forces besides the external forcing (i.e., $\mathbf{F}$). This can be accomplished by either adopting the ''tau approximation,''

$$\mathbf{D}_{\rm damp}\equiv-\frac{\mathbf{v}}{\tau} \tag{4}$$

for some constant τ or, alternatively, by introducing viscosity damping, e.g.,

$$\mathbf{D}_{\rm damp}\equiv\nu\nabla^2\mathbf{v}, \tag{5}$$

the latter being understood in the Lagrangian sense: the derivatives are taken *in situ*, that is, on the field line. Then by properly choosing the forcing, and specifying the values of either τ or ν, it is possible to generate any desired motion with given amplitude. Most of the simulations presented here, however, are based on damping of the form (4), for both STF and ABC flows; the only case when Eq. (5) is used corresponds to the calculation of both velocity and magnetic spectra in Sec. V B. We will return to the discussion of the damping terms later in this section.

Up to this point, the problem must be considered as kinematic: although the velocity field is no longer given, and obeys the Newton law (3), the backreaction of the magnetic field is not taken into account. Nevertheless, in this kinematic regime, the velocity field following from Eq. (3) is more realistic than an arbitrary, ad hoc, imposed flow. For example, one could ask if an actual velocity field of STF or *ABC* form can be constructed so as to satisfy the Newton law; we consider this question in Secs. III and V A.

In order to reach a more complete (i.e., dynamical) description, we need to include the Lorentz force in the momentum equation. We shall do this, subject to the following two assumptions:

(1) As in [11], we shall delay only with one, or a few, field lines; one can therefore account for field line tension in the evolution equations by writing

$$\mathbf{F}_B \equiv -\frac{1}{4\pi\rho}\frac{B^2}{r^2}\mathbf{r}, \tag{6}$$

where $\mathbf{r}$ is the principal vector normal to the curve.

(2) We shall only consider incompressible flows. For this reason, the forcing term $\mathbf{F}$ is chosen to be incompressible, so that the generated velocity field is incompressible as well, and the potential part of the Lorentz force (i.e., the gradient of the magnetic pressure) is supposed to be compensated by thermal pressure.

Given these assumptions, Eq. (3) reads

$$\frac{d\mathbf{v}}{dt} = \mathbf{F} + \mathbf{D} - \frac{1}{4\pi\rho}\frac{B^2}{r^2}\mathbf{r}. \tag{7}$$

The model dynamical equation (7) is strikingly similar to the Lagrangian momentum equation. In addition, all simulations are done in Lagrangian coordinates; i.e., we follow the field line trajectories. To be more specific, we shall follow either a family of trajectories, starting with initial points placed on an initial field line, or (in other experiments) we shall follow several families of trajectories, starting on several magnetic field lines.

The magnetic field is calculated by using the Lagrangian approach as well. As in [11], the field is defined in terms of the Lundquist solution,

$$\frac{\mathbf{B}(\mathbf{x},t)}{B(\mathbf{a})} = \frac{d\mathbf{s}}{ds(t=0)}, \tag{8}$$

where $d\mathbf{s}$ is an infinitesimal vector connecting two neighboring liquid particles, and $\mathbf{x}$ is the final position of the particle at the end of the trajectory, assuming it started at position $\mathbf{a}$. Solving Eqs. (7) and (8) makes it possible to perform nonlinear calculations in three dimensions (3D), with apparently infinite magnetic Reynolds number (since we are using the Lundquist solution for the ideal problem).

In addition, as pointed out in [11], it is possible to define an effective R_m, even for an ideal problem, as follows (see also Sec. I):

$$R_m \equiv \left(\frac{l}{\delta}\right)^2, \tag{9}$$

where l (the flow scale length) and δ (the correlation length of the magnetic field) are both mathematically well-defined quantities. Note that δ must be well resolved by the numerical integration; this latter condition is necessary so that the effective Reynolds number is defined by Eq. (9) rather than being limited by the numerical accuracy of the integration. As we shall show in the next section, this effective magnetic Reynolds number allows us to investigate the contribution of small-scale motions to the evolution of large magnetic scales. We further note that the effective Reynolds number reaches values of approximately 10^4 in [11], and in the nonlinear case discussed below it reaches even larger values (cf. Sec. IV). Furthermore, as mentioned in Sec. I, solution of the full MHD is usually restricted to modest values of R_m; the solutions easily become unstable for large values of R_m. The latter undesirable behavior does not arise if one uses the Lagrangian approach [i.e., Eqs. (7) and (8)].

An important question about our model dynamics is to what extent it captures the dynamical processes likely to be important in the full problem. Thus, models such as ours often used for dynamos cannot account for phenomena such as shear flow instabilities, usually because of the strong imposed forcing: the latter is time dependent, and it actually does not allow time enough for instabilities to develop; but it is readily shown that the model can simulate (for example) Alfvén waves. In fact, it is an ensemble of Alfvén waves that appears in the fully developed nonlinear regime we shall be studying.

Because nonlinear effects generally result in the smoothing of magnetic field lines, our simulations are subject to a surprising simplification: the increased smoothness of magnetic field lines in this limit allows one to carry out simulations for much longer times. This is because, in the dynamic limit, the field structure does not continue to become more and more convoluted as the calculation proceeds, and therefore the field geometry remains spatially fully resolved. [We recall from [11] that the field is considered to be well resolved if the distance between the neighboring points remains small when compared to the smallest physical scale δ; only then is the definition of the magnetic field based on Eq. (8) reliable.] Indeed, we find that in the nonlinear regime, the field strength does not (in a statistical sense) grow in time, i.e., the distance between two neighboring points on a given field line remains statistically constant. As a result, we are able to compute field line trajectories for much longer times in the nonlinear case than in the linear regime.

Another important consideration in nonlinear calculations is related to the damping forces. As already mentioned, the forces given by Eqs. (4) and (5) are added in the kinematic regime in order to make sure that there is no secular growth of kinetic energy. Simple estimation of these damping terms in the nonlinear regime shows, however, that they are negligible when compared with the other terms; that is, the external forcing $\mathbf{F}$ in Eq. (7) is balanced mainly by the magnetic tension $\mathbf{F}_B$. This is especially true for viscous forcing in the form Eq. (5). For example, when studying the spectrum, Sec. V B, we examined the stability of solutions for very small values of ν; thus, we decreased ν to values of order 0.000 03, and found that the solution remained stable. Unfortunately, this result cannot be interpreted to mean that we have solved the problem for very large Reynolds numbers because, as just mentioned, the viscous term is simply small, and does not play any important role in the nonlinear stage; stability is instead ensured by the time-dependent forcing.

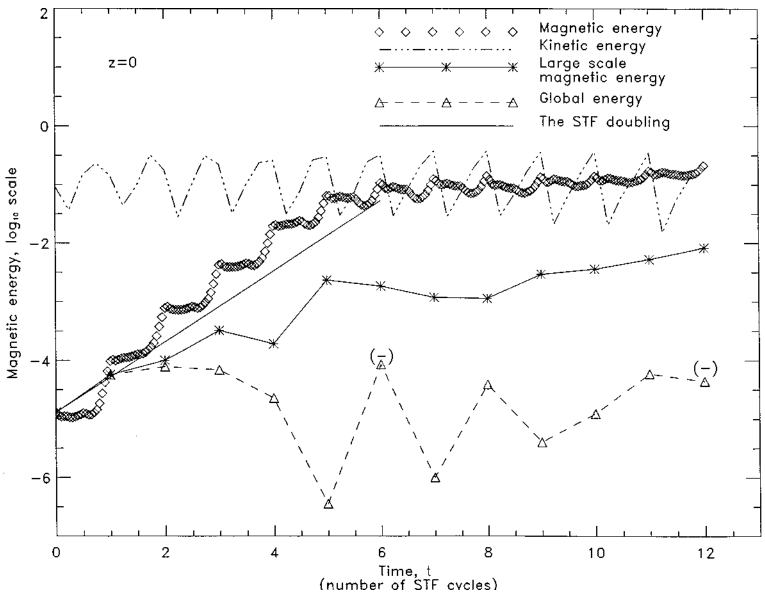

FIG. 1. Evolution of magnetic and kinetic energies for a magnetic field line that started in the $z=0$ plane.

III. THE STRETCH-TWIST-FOLD: KINEMATIC APPROACH

As a starting point, we consider again the kinematic problem discussed in our first paper [11], but now based on the case of the model dynamic equation (3), with damping based on Eqs. (4) or (5). To begin with, we note that if the forcing is chosen in such a way that the forced motion performs the continuous STF cycle, the results of [11] are duplicated. That is, this forced STF flow results in a simple doubling of field line loops, as was expected before we presented our earlier calculations [11], only for a few ''favored'' field lines, and only for a limited number of the STF cycles. In the present case, it is necessary to very carefully tune the parameters for the forcing, rather than for the velocity itself, in order to achieve this simple ''expected'' result for only a few selected field lines. (Most other field lines of course behave drastically differently.) As a result, essentially all field lines again end up behaving chaotically after roughly four STF cycles, while the ''favored'' lines behave in a ''proper'' manner only for a few cycles, and then also become chaotic. This field line chaos suggests the presence of a high level of magnetic fluctuations.

As an illustration, we consider two initial lines, the first a circle with radius $r=0.51$ placed in the $z=0$ plane, and the second (with the same radius) placed in the $z=0.1$ plane. The first field line is ''favored,'' and therefore (as seen in Fig. 1) the associated magnetic energy grows as expected, at least for a few cycles; in the case of the second line, the associated magnetic energy grows substantially faster (Fig. 2).

In order to measure the parameter n [cf. Eq. (1)], we must measure the following quantities: (i) the magnetic energy $\langle B^2\rangle$, which is easy to calculate; (ii) the large-scale magnetic energy $\langle B_0^2\rangle$, which is nontrivial to compute because of the chaotic and highly irregular field structure; (iii) the effective magnetic Reynolds number, which we defined earlier via Eq. (9). (As an aside, we note that while the large-scale scale length l is mathematically well defined, it can be somewhat ambiguous to measure; this is because the magnetic field has a tendency to expand spatially as amplification proceeds, so that l grows secularly.)

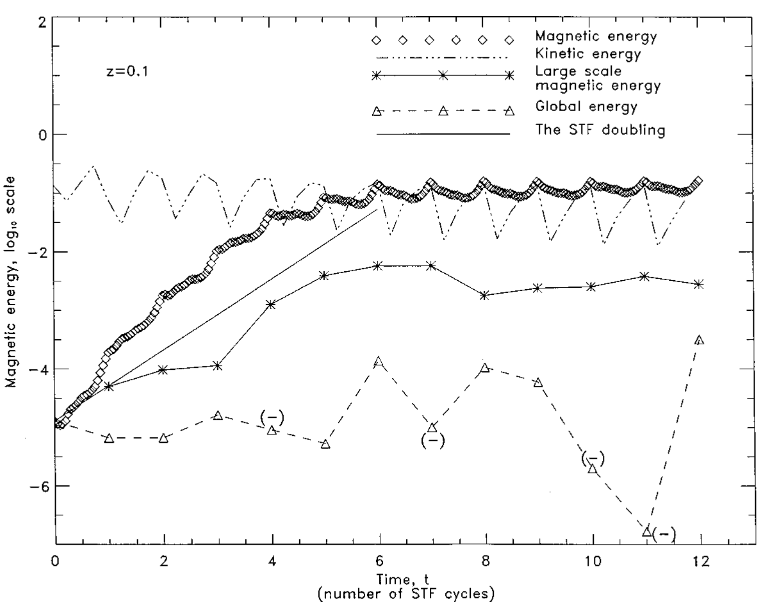

FIG. 2. Same As Fig. 1, but for a magnetic field line starting in the $z=0.1$ plane.

Note that the parameter n depends only logarithmically on the parameters mentioned above, and can be defined easily if one can demonstrate scaling with the Reynolds number R_m; using this approach, we were able to estimate n with relatively good accuracy in our earlier calculations [11], based on more than three decades of scaling. We shall take advantage of these earlier results when comparing with the present calculations, which are focused primarily on the nonlinear dynamics.

Returning to the large-scale magnetic field component [which is related to point (ii) above], we recall that in [11] B_0 was defined in terms of the long-range portion of the correlation function. The latter was constructed along field lines. In the present calculations, we also measure the ''circulation'' or, more precisely,

$$\Phi = \langle B_\phi \rangle. \tag{10}$$

This quantity is computed as an average over all points, and therefore can be computed fairly reliably (in contrast to the large-scale field derived from the field correlation function, which we focused on in our earlier calculations [11]). In order to understand the meaning of Φ, we note that if the STF would have resulted in simple doubling of magnetic loops, then $\Phi = \Phi(0)2^m$, where m is the number of the STF cycles, and therefore

$$\Phi^2 = \Phi(0)^2 2^{2m}. \tag{11}$$

We will refer to the quantity Φ^2 as the ''global'' magnetic energy (as opposed to the large-scale magnetic energy, defined from along-field-lines correlations), and will use it exclusively in the following. We prefer to use the circulation Φ as a measure of the large-scale magnetic energy because it is easily and reliably commutated, and because the results derived indeed recover the expected properties of large-scale mean fields. For example, if one were to compute any average magnetic field component other than $\langle B_\phi \rangle$, then the expected result should be zero. Thus, one would expect that $\langle B_x \rangle = 0$ exactly. In simulations, however, such quantities never vanish exactly, but should be very small, e.g., of the order of the round-off errors. Indeed, we find that while the computed $\langle B_\phi \rangle \sim O(1)$, the computed components such as $\langle B_x \rangle \sim O(10^{-9})$, many orders of magnitude smaller than $\langle B_\phi \rangle$. Thus, the computed circulation is always well above the noise, and can be well measured.

We end this section by noting a surprising (and discouraging) result that appears even at the level of this kinematic description: even cursory examination of the evolution of the large-scale magnetic energy (seen in Fig. 1 for the case of a field line starting from the $z = 0$ plane) shows that the global energy grows rapidly only after the first cycle (as expected from the construction: recall that we are dealing with one of the ''favored'' field lines), and that soon after (but well before one enters the dynamic regime), the global energy grows more slowly, and finally stops growing. If one examines the corresponding evolution for the field line that started from the $z = 0.1$ plane (Fig. 2), one sees that its associated global energy does not grow at all. These results suggest that the STF motion does not really work as was previously expected even in the kinematic regime, i.e., the circulation (or magnetic moment) does not grow after all; yet, nevertheless, there are large-scale structures in the field that do grow, as seen from Figs. 1 and 2, and therefore we must conclude that a large-scale dynamo is realized by this (STF) motion. The question is how we can understand this behavior, especially as one enters the dynamic regime. We explore this question in the next section.

IV. THE STRETCH-TWIST-FOLD: THE NONLINEAR STAGE

In this section, we shall consider in some detail the nonlinear behavior of the STF dynamo. To begin this discussion, we note once again that in the kinematic regime we based our discussions on measurements of two quantities (B_0 and l) that were themselves not well defined, but because of the range of values of the Reynolds number R_m that was explored, we were able to recover meaningful scaling results with R_m [11]. In the present case, we shall not be able to rely upon calculations with such a wide range in Reynolds numbers, and will therefore need to adopt a different strategy for deciding the properties of the dynamo-produced fields. In particular, we have adopted a slightly different definition for the large-scale field (as discussed immediately above), which allows us to investigate the field characteristics by examining the multifractal structure of the growing magnetic fields.

As discussed earlier, one of the keys to reaching such an understanding is to estimate the parameter n, defined in Eq. (1); in principle, one would expect that we would have to determine all of the quantities (i)–(iii) listed in Sec. III in order to construct this estimate. However, in the nonlinear regime we know that the magnetic Reynolds number [defined by Eq. (9)] reaches some asymptotic value because both the large-scale length scale l and the diffusive scale δ themselves reach asymptotic values as the calculation proceeds. In other words, one must conduct a large number of simulations in order to build up the statistics for determining n in this manner. In contrast, there exists a less computer-intense method for determining n, based on a study of the detailed spatial structure of magnetic field lines acted upon by the STF flow. We discuss this in the following section.

A. The large-scale magnetic field

Our simulations were carried out with a magnetic Mach number

$$M_A = \frac{4\pi\rho\langle v^2\rangle^{1/2}}{\langle B(t=0)^2\rangle^{1/2}} = 10^2,$$

so that the initial magnetic energy is four orders of magnitude below the kinetic energy. As seen from Figs. 1 and 2, all quantities saturate after approximately five STF cycles. As mentioned in Sec. II, the distance between neighboring particles on a given field line does not grow in the nonlinear regime; this property of the nonlinear regimes has the happy consequence that we do not lose spatial resolution for relatively long times when compared to the kinematic approach. Specifically, it was possible to proceed up to only six STF cycles in the linear calculations presented in [11], while in the nonlinear regime discussed here we are able to compute up to 12 cycles.

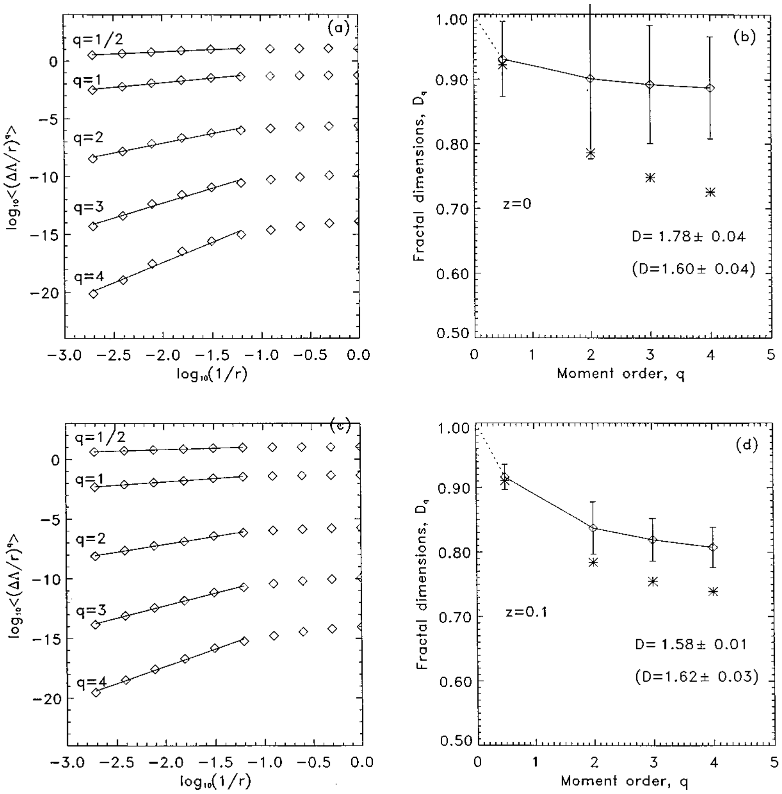

FIG. 3. Multifractal dimensions of the magnetic field line length. (a) Scaling for an initial magnetic field line lying in the $z=0$ plane. (b) The corresponding dimension spectrum D_q. For comparison, we also show the corresponding spectrum for the kinematic STF [11] (asterisks). D is the classical line dimension; we provide (in parentheses) the dimensions previously obtained for the kinematic case. Panels (c) and (d) are the same as (a) and (b), respectively, but for an initial field line that lies in the $z=0.1$ plane.

A few features of the results in this nonlinear regime are worthy of note. First, we observe that the circulation Φ can change sign [as marked with a $(-)$ sign in Figs. 1 and 2]. This is of relatively little consequence, as it only means that the magnetic loop turns around from its original orientation, and thus the magnetic moment changes sign.

Of substantially greater significance is the fact that the global energy does not grow in the long time limit, independent of where the original field line was started; i.e., this result holds for field lines started both in the $z=0$ and the $z=0.1$ planes. For example, the first field line—which is "favored"—does show, at least initially (when the kinematic approach is still valid), that the associated global field grows (see previous section). However, after a few cycles, the energy in this case is seen to even diminish (Fig. 1), leading to the pessimistic conclusion that nonlinear effects may totally kill field line doubling.

However, the large-scale field, when calculated along the field line, does grow in time, and its associated energy saturates at a level about two magnitudes below the value of the total magnetic energy. Note that the kinetic energy does not really change with time. These results support the idea that nonlinear effects in the dynamo do not suppress the turbulence as such, but rather suppress the transport coefficients (such as the diffusion and generation coefficients) responsible for the large-scale field amplitude [8].

B. Fractal structure of magnetic field lines

As in [11], we consider next the multifractal properties of the field lines. The generalized dimensions are defined as

$$\left\langle \left(\frac{\Delta\Lambda}{\Delta s} \right)^q \right\rangle \sim \left(\frac{1}{\Delta s} \right)^{\kappa q + (1-D_q)(q-1)}, \tag{12}$$

where $\Delta\Lambda$ is the distance between two points on a given field line (whose initial separation is given by Δs), and the fractal (or generalized) dimensions are denoted by D_q. Note that by setting $q=1$, we recover the classical definition of the fractal length dimension; thus, if $\langle \Delta\Lambda/\Delta s \rangle$ shows scaling properties, then κ can be found. The Richardson-Mandelbrot dimension D is then given by

$$D=1+\kappa. \tag{13}$$

After computing κ, all other dimensions D_q can be found from any extant scaling of $\langle (\Delta\Lambda/\Delta s)^q \rangle$; indeed, as shown in Fig. 3, we do find scaling for roughly 1.5 decades. Recall that if the multifractal dimensions of a curve are not equal to unity, it is implied that the field line is stretched (statistically) inhomogeneously. As seen from Figs. 3(b) and 3(d), the dimensions D_q are systematically greater in the nonlinear regime than in the kinematic STF regime. In other words, they are closer to the trivial dimension, $D_q=1$; indeed, the error bars are sufficiently large for the field line initially lying in the $z=0$ plane [Fig. 3(b)] that the dimensions D_q shown are consistent with the trivial case.

This increase of dimensions can be easily understood: The STF stretches the field lines inhomogeneously and, as a result, the field line becomes multifractal. On the other hand, the field line tension tends to smooth out the inhomogeneities, and as a result of this second effect, the field line becomes less singular as one enters the nonlinear regime.

Our computation of the classical dimension D is also well determined, as can be seen from the relatively small error bars shown in Fig. 3. The field line initially lying in the $z=0$ plane becomes more singular, that is, its classical dimension D is larger than its value for the kinematic case, while the field line starting from the $z=0.1$ plane is roughly

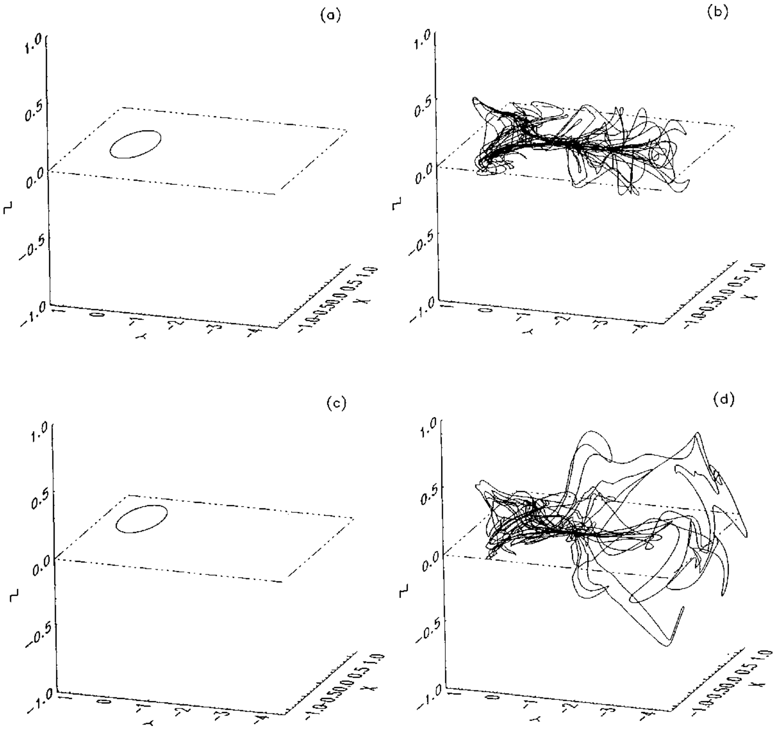

FIG. 4. Evolution of a magnetic field line. Panel (a) shows the magnetic field line at the start (i.e., as a circle lying in the $z=0$ plane); panel (b) shows the same field line after 12 STF cycles. Panels (c) and (d) are the same as (a) and (b), respectively, but for an initial field line lying in the $z=0.1$ plane.

as singular as in the kinematic regime. This behavior can be understood by noting that there are two competing effects:

(i) As already noted, the line is stretched more homogeneously in the nonlinear regime. That is, instead of having very complicated small-scale structure, highly stretched in only some places, i.e., in a very intermittent fashion (as is the case in the kinematic regime), the line becomes stretched everywhere in the present dynamical regime. As a result, its length increases.

(ii) The nonlinear forces limit the line stretching as a whole: the magnetic field cannot grow indefinitely in the dynamic regime. This limits the total length of the line.

More quantitatively, these two requirements follow from the inequality (2.20) presented in Ref. [14],

$$\kappa \leqslant D_\infty . \tag{14}$$

For a very intermittent process, such as the one described in [11], D_∞ is substantially less than unity, and therefore κ, as well as the dimension D, by Eq. (13), have to be small. In other words, very singular processes in terms of intermittency result in reducing the singularity of the length. In the nonlinear regime, the intermittency is reduced, i.e., $D_\infty \lesssim 1$, and κ is therefore allowed to become greater; that is, the line could be more singular as far as its length is concerned.

The corresponding field lines are depicted in Fig. 4. Panels (b) and (d) show the field lines after 12 STF cycles. We can see that the lines do not even barely resemble circles, but nevertheless are not as complicated as compared to the results of the kinematic regime. As explained above, this is due to the smoothing by Lorentz forces. Another way of illustrating the growing geometric complexity of the magnetic field as the STF process proceeds is to plot the $\{r,z\}$ coordinates of all of the computed points along a given field line (as shown and described in Fig. 5), after 12 STF cycles. (This figure is an analog of the polarized Poincaré map introduced in [11].) In order to appreciate what actually occurs, it is useful to consider what one would naively expect to happen. Thus, for an initial magnetic field line starting in the $z=0$ plane, we know that all of the points on this line are represented by dots, which are all placed on top of each other at $\{r=0.51,z=0\}$; there are no pluses. After several STF cycles, we would expect (according to [6]) a ''cloud'' of dots located near the initial radial value $r=0.51$, and slightly spread in the vertical dimension (z). Again, we would not expect any pluses because the field line is not supposed to reverse, i.e., the naive STF model assumes that B_ϕ does not change its sign as the STF cycle proceeds. It is clear from Fig. 5(a), however, that this simple picture is incorrect: The field line is chaotic, and does go in the opposite direction; i.e., B_ϕ does change its sign as the STF cycle proceeds. (Indeed, one observes more pluses than dots, but this result is obtained because the circulation changed sign for this particular case; see Fig. 1). Similar considerations apply to the case of a line starting in the $z=0.1$ plane: its initial map would look like that for the $z=0$ line, except all points (and all dots) would be lying on top of each other at $(r=0.15,z=0.1)$; and one would again naively assume that after the application of the STF process, the ''cloud'' of dots should be centered around this point. As seen from Fig. 5(b), this is again not the case. Thus, despite the fact that the nonlinear regime has a tendency to reduce the convolute evolution of any given field line, it is still true that the actual end result of the STF process is a field geometry that does not at all resemble what one would expect on the basis of the classical STF continuous ''doubling'' of circular field lines.

We now proceed to the estimation of parameter n discussed in Sec. I [e.g., Eq. (1)]. Nonlinear calculations do not provide any scaling for the ratio $\langle B^2\rangle/\langle B_0^2\rangle$, and therefore we can obtain only a rough estimate for n. Indeed, as seen from Fig. 6, the values of n thus obtained (i.e., from line correlations) show a wide range. In particular, these values are com-

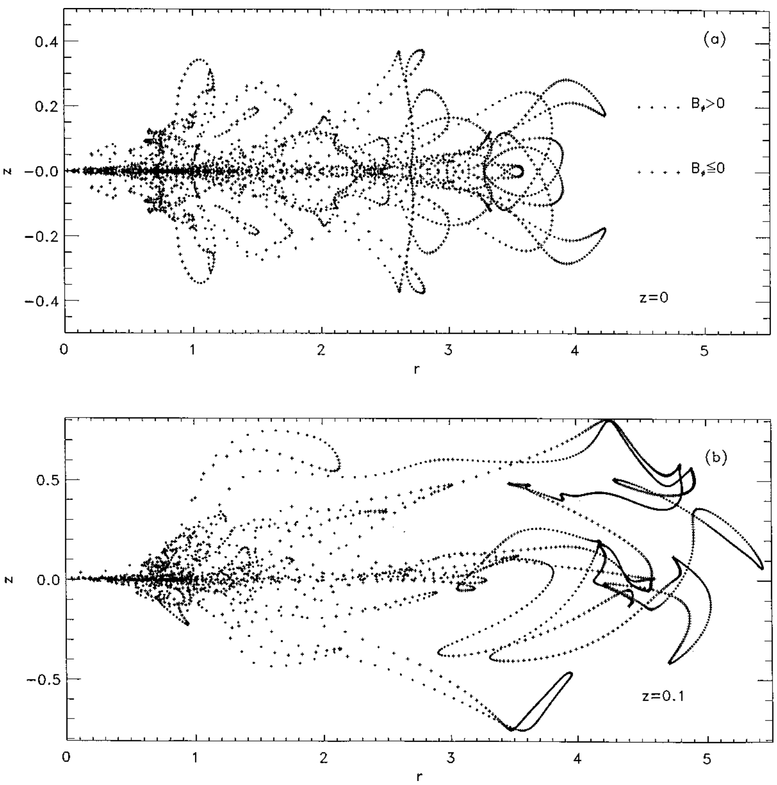

FIG. 5. Illustration of the geometric complexity of STF-distorted field lines. We show, for the case of two field lines (located initially at $z=0$ and $z=0.1$) distorted after 12 STF cycles, the location in the $\{r,z\}$ plane of every computed point along each field line; this is an analog to the polarized Poincaré maps discussed in [11]. In order to retain some sense of the field line orientation, we coded each such point according to the sign of the field component B_ϕ at that point: we use a dot for all points where $B_\phi > 0$, and a plus otherwise. Panel (a) shows what happens to a field line starting in the $z=0$ plane; (b) shows the same result for a field line starting in the $z=0.1$ plane.

pletely unreliable when calculated for a field line after few STF cycles: the lines are actually not chaotic, and therefore there is insufficient statistical data to actually compute a reliable value for n. Nevertheless, there is some indication that the ''average'' value of n computed in this manner is around unity; i.e., it is definitely bigger than in the kinematic limit.

In order to obtain a more reliable estimation for n, we define this parameter using the formula

$$n = \kappa + \frac{1 - D_2}{2} \tag{15}$$

[15]. Each quantity in Eq. (15) can be obtained from scaling laws, which is why this definition is relatively more reliable for computing n. Indeed, this quantity can be seen to behave more realistically [cf. Fig. 6(b)]: it starts from very small

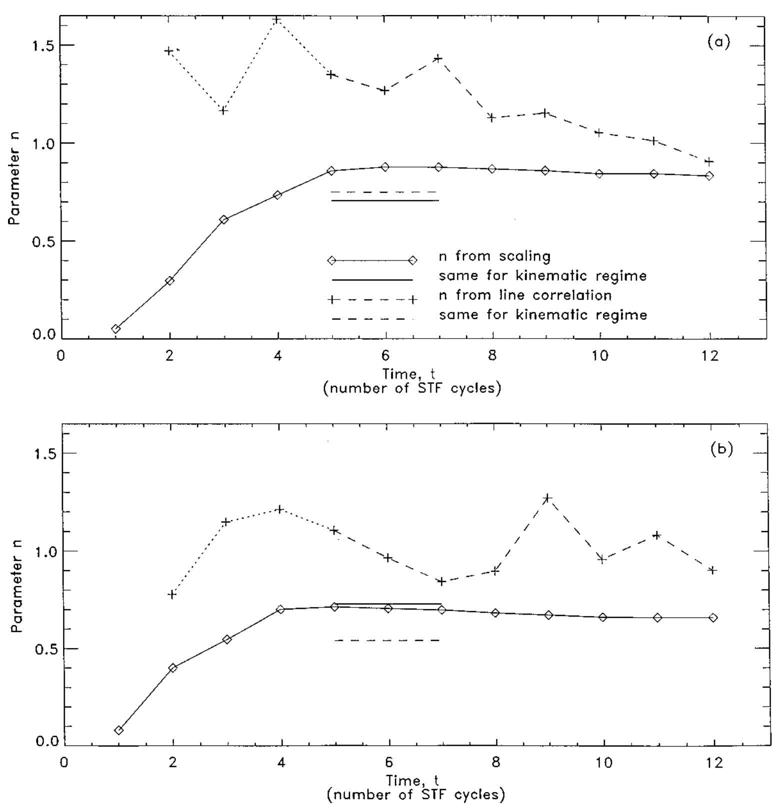

FIG. 6. The exponent n as calculated in various ways, for (a) line starting in the $z=0$ plane, and the same (b) for a line starting in the $z=0.1$ plane. The notation conventions are the same in both panels. Dotted sections of the lines (indicated by pluses) correspond to regions on these field lines where our calculations tend to give unreliable results.

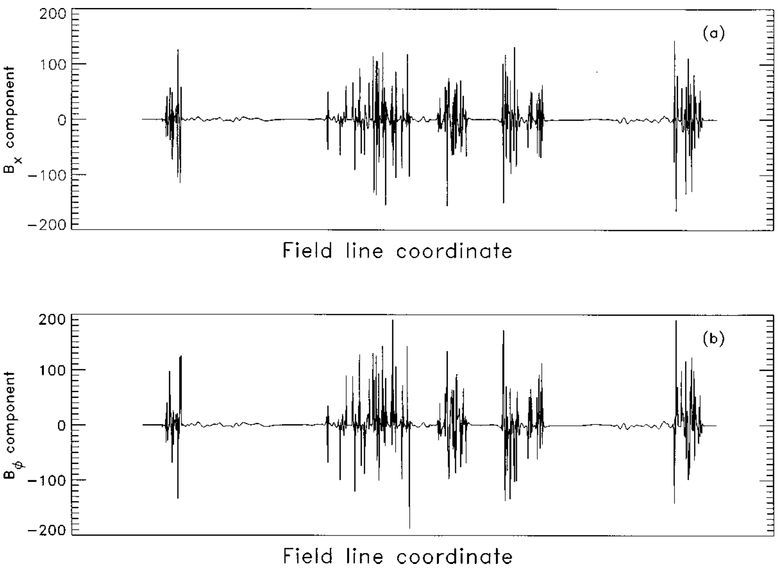

FIG. 7. Plots of the B_x component (a) and B_ϕ component (b) along the field line that started in the $z=0.1$ plane, but after 12 STF cycles.

values, increases, and reaches some asymptotic value. While these values still fall below those obtained from the line correlation (which we regard as relatively unreliable), they are still larger than those obtained in the kinematic limit. However, there remains an ambiguity: if we calculate n in the kinematic regime not using the procedures described in [11], but via formula (15), i.e., through scaling, then for the line shown in Fig. 6(b) we obtain a value for n that is slightly larger than for the nonlinear case. In order to resolve this discrepancy, we note that the value of n for the $z=0.1$ line was obtained with considerable uncertainty: in particular, the scaling was quite poor [cf. Fig. 10(d) of [11]]. Therefore, if we accept the new value of $n=0.73$ for the kinematic regime, then it appears that the value of n may diminish in the nonlinear regime when compared to the kinematic [see Fig. 6(b)].

This reduction was indeed expected (cf. Sec. I). However, the line initially in the $z=0$ plane does not show this expected behavior: the value of n computed for this case increases in the nonlinear limit; and this increase is actually more convincing [cf. Fig. 6(a)] than the decrease [cf. Fig. 6(b)]. Our previous discussions have shown how this seemingly puzzling conclusion can be reconciled with our earlier result. In particular, we need to go back to the two points (i) and (ii) discussed in the earlier subsection. If we translate the effects of nonlinear backreaction on the field line length (and stretching) to the implied magnetic field properties, we conclude the following. (i) It is clear that a very intermittent field (in the kinematic regime) has a small filling factor, and therefore the value of $\langle B^2 \rangle$ is substantially smaller than the typical field energy. If we smooth out this field (which is what happens in the nonlinear regime), this average increases. That is why this parameter n might increase.

(ii) On the other hand, the same nonlinear backreaction limits the magnetic energy, which would result in a decrease of n.

As we see from the simulations, these effects compete; sometimes one effect wins out over the other and sometimes it is the reverse.

At this point, we finally are able to estimate the effective magnetic Reynolds number directly from formula (1), where all the quantities entering into this formula are obtained through reliable scaling. We then obtain (in the nonlinear regime) $R_m = 11\,966$ for the line starting in the $z=0$ plane, and $R_m = 36\,913$ for the line starting from the $z=0.1$ plane.

C. The small-scale structure of magnetic field

Next we consider the intermittency properties of the magnetic field, if any. As stressed above more than once, the nonlinear effects reduce intermittency, while we know that the field is quite intermittent in the kinematic regime [11].

Figure 7 gives some idea of how intermittent the magnetic field is for the case of a field line started in the $z=0.1$ plane, and after 12 STF cycles. It depicts the B_x component [Fig. 7(a)] and the B_ϕ component [Fig. 7(b)], both computed along the field line. Both components are normalized to the initial field strength. In other words, the initial B_x component would be a sinusoid with amplitude equal to unity, and hence would be indistinguishable from the zero line on this plot. The initial B_ϕ would also be represented by the $y=1$ line, i.e., would be again indistinguishable from zero.

The two curves in Fig. 7 look quite similar. However, differences appear if one calculates the mean value. For the first curve [Fig. 7(a)], the mean is 8.1×10^{-8}, i.e., practically zero (within round-off errors), while for the B_ϕ curve in Fig. 7(b) the mean is 1.41. This result was already alluded to in Sec. III: the mean of B_ϕ (actually, the circulation) is indeed a reliably computed quantity.

These plots are similar in the sense that both reveal quite intermittent structures. Indeed, the flatness factor

$$f=\frac{\langle B^4 \rangle}{\langle B^2 \rangle^2}$$

is 7.97 for this magnetic field. The flatness is substantial, when compared with Gaussian value 3, although small compared with kinematic case (the flatness was 258.4). Thus, nonlinear effects do decrease intermittency, although it remains substantial.

For this reason, it makes sense to measure intermittency fractals. We measured correlations of magnitudes, as in [11], and used the formula

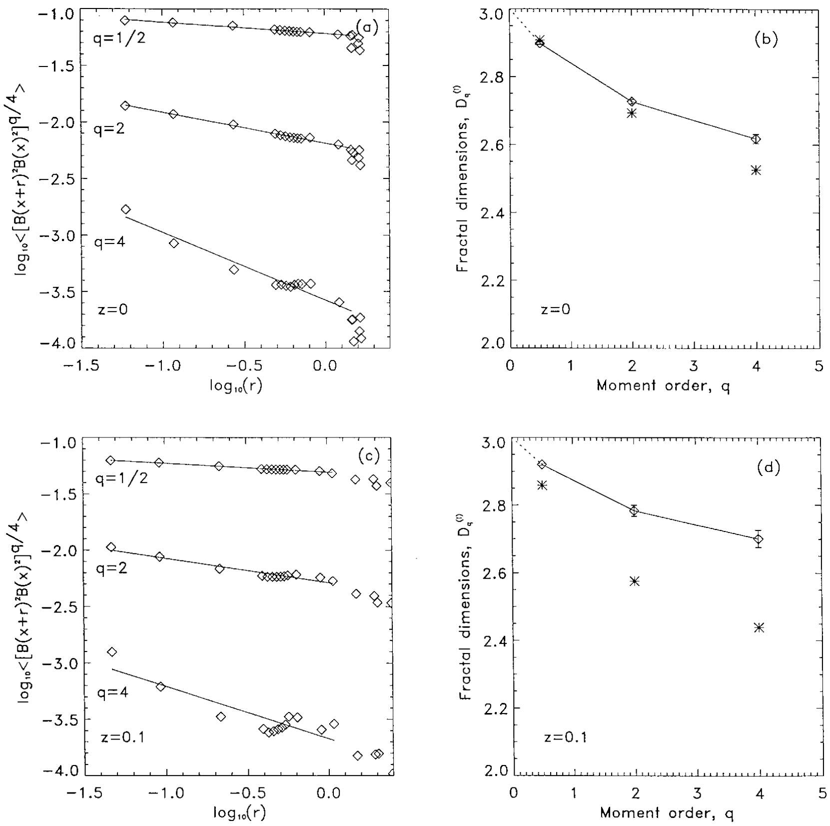

FIG. 8. Intermittency fractals of the magnetic field after 12 STF cycles. Panel (a) shows the scaling, and panel (b) the corresponding fractal dimensions $D_q^{(i)}$; both results are obtained for a line that started initially in the $z=0$ plane. Panels (c) and (d) are the same as (a) and (b), respectively, but for an initial field line lying in the $z=0.1$ plane. For comparison, we also show previously obtained spectra for the kinematic STF [11] (asterisks).

$$\langle[\mathbf{B}(\mathbf{x}+\mathbf{r})^2\mathbf{B}(\mathbf{x})^2]^{1/4}\rangle \sim r^{(3-D_{q/2}^{(i)})(q/2-1)2-(3-D_q^{(i)})(q-1)}; \tag{16}$$

here the generalized dimensions $D_q^{(i)}$ are based on the measure

$$\mu(C)=\frac{\int_{C_i}|\mathbf{B}|d\mathbf{x}}{\int_V|\mathbf{B}|d\mathbf{x}},$$

where the total volume V is divided exhaustively into disjoint subsets C_i.

Figure 8 shows the scaling and generalized dimension spectrum for two lines: one starting in the $z=0$ plane, and the other one in the $z=0.1$ plane. We can see that the dimensions are systematically bigger in the nonlinear regime as compared to the kinematic case. This trend is quite robust, and definitely above the noise; one can compare this result with what is shown in Fig. 3, where a similar trend is observed as well, but not as pronounced. As above, this trend can be explained by appealing to the nonlinear smoothing of magnetic inhomogeneities—the magnetic field becomes less singular.

V. THE FORCED *ABC* FLOW

In order to understand the properties of the STF flow better, we shall now compare the earlier results with what one finds upon examining the nonlinear response of a system in which the underlying flow is the so-called ABC flow (cf. [3]).

Whereas one usually prescribes the ABC flow, i.e., one is given the flow

$$v_x=A\ \sin kz+C\ \cos ky,\quad v_y=B\ \sin kx+A\ \cos kz,$$

$$v_z=C\ \sin ky+B\ \cos kx, \tag{17}$$

we shall instead impose a forcing function (following the discussion of Sec. III) such that the flow (17) appears. Unsurprisingly, the forcing necessary to accomplish this must itself have the form of Eq. (17).

If the coefficients A, B, C are constants, then the flow is laminar in the Eulerian sense, but it is well known to exhibit Lagrangian chaos (see, e.g., [3]), which is referred to as ''Lagrangian turbulence.'' We are interested, however, in true turbulence, and therefore choose these coefficients as random functions in time: specifically, we consider them uniformly distributed on the interval [0,1]. The wave vectors is fixed, $k=10$, corresponding to a characteristic scale $\pi/10=0.31$.

The flow is not random in space, but is rather periodic in space, and random in time. If a very weak magnetic field is imposed, we would expect two effects. First, the field should be diffused by turbulent diffusion; second, a large-scale field component might be generated by helical turbulence. The turbulence is indeed helical because one can readily show that

$$\langle\mathbf{v}\cdot\nabla\times\mathbf{v}\rangle=\langle A^2+B^2+C^2\rangle k\neq 0,$$

and therefore field generation is possible via the so-called alpha effect (see, e.g., [16]). In addition, a small-scale dynamo is also possible, i.e., the generation of a small-scale component of the magnetic field, which is more effective than scale reduction (see [6,11]).

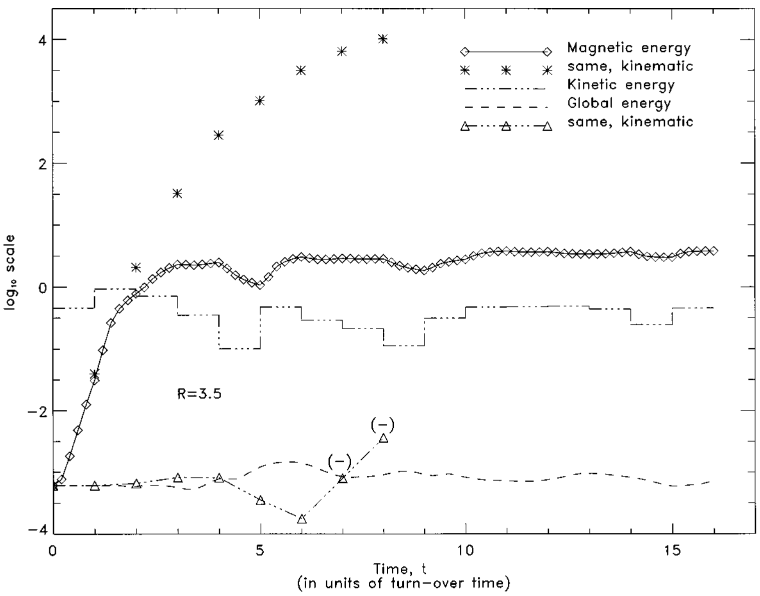

FIG. 9. Evolution of magnetic and kinetic energies for both kinematic and dynamic cases (as in Fig. 1) for the case of *ABC* flowlike forcing.

A. Kinematic approximation

If the velocity field is defined by either Eq. (4) or Eq. (5), then the magnetic field is found from Eq. (8). We investigated a large number of cases, with a variety of different parameters; the forcing used was always of the form (17). The initial field was represented either by a single field line lying in the $z=0$ plane, characterized by a circle centered at the origin of radius $R=1$ or $R=3.5$, or by several lines, all circles also lying in the $z=0$ plane, with radii $R=1$, 2, 3, 4, 5, respectively. Qualitatively, the flow always results in a high level of fluctuations: this is not a new result, and is well known for the *ABC* flow (see, e.g., [3,4]). As one example, Fig. 9 illustrates the results of this type of calculation. The magnetic energy in the kinematic approach grows exponentially (as denoted by asterisks). Note that during the last few turnover times, the energy growth seems to slow down; however, this is an artifact of the calculation because we are simply starting to run out of spatial resolution at these later stages (i.e., the distance between two neighboring points on a field line begins to be too large for the formula (8)—which assumes infinitesimal distances—to be valid).

As for the global energy, it does not grow at all and, at two late stages, the flux changes sign (see Fig. 9). The large-scale energy, which is calculated via the line-of-force correlations, is practically zero except for the first two cycles: in the initial stage, because it is defined as a circle, and the next stage, because there is not enough time as yet to change the field configuration drastically. Thus, there is no large-scale dynamo in that case. There are some indications, though, that the field does grow on scales comparable with the flow scale; i.e., with $\pi/k=0.31$, we would not consider this scale ''large.'' The ratio $\langle B^2\rangle/\langle B_0^2\rangle$ attains an amplification of six orders of magnitudes, and so the level of fluctuations is indeed high.

The alpha effect does not seem to work in this case, presumably because it has to compete with turbulent diffusion (see, e.g., [17]), and apparently fails to win. The latter process, i.e., turbulent diffusion, is indeed present, and will be discussed further below.

The small-scale magnetic field is essentially nonintermittent in this case. Indeed, measuring fractal length dimensions by formula (12) results in $D_q \lesssim 1$, and the difference between D_q and unity is within the noise. But the scaling itself is good for about 5 decades. Therefore, following a construction analogous to Fig. 3(a) should result in much better scaling, but all plots (except for $q=1$) lead to trivial generalized dimensions. Figure 10(a) depicts such a scaling for $q=1$, with nontrivial dimension $D=1.92\pm0.01$, corresponding to a measurement at $t=8$ (t measured in units of the turnover time).

The temporal evolution of this dimension and of the parameter n are depicted in Fig. 10(b) (analogous to Fig. 6). Note the very small error bars, resulting from the large scaling range. The parameter n is calculated from formula (15). The curve is rather singular, the dimension D being substantially bigger than unity, although the length is not intermittent. It means that the field line is ''homogeneously singular.''

We also constructed intermittency fractal dimensions, via Eq. (16), analogous to Fig. 8. The scaling is again good, but the deviations of the dimensions $D_q^{(i)}$ from unity are within the noise. The actual absence of intermittency can be explained as follows. Unlike the STF motion, which stretches the field line quite inhomogeneously, the *ABC* motion is periodic, and if the spatial scale of the magnetic field is much bigger than that of the velocity (which is the case in these simulations), then on average one would expect the field line to be stretched homogeneously.

B. Nonlinear stage

We also carried out a large number of simulations using momentum equations (4), or (5), for a variety of parameters. One example is illustrated in Fig. 9. The initial field line is a circle with radius 3.5, and the initial Mach number is $M_A^2=1632$ (so that the initial magnetic energy is 0.06% that of the kinetic case). After a few turnover times, the field is saturated. The global field remains more or less steady, and does not change sign.

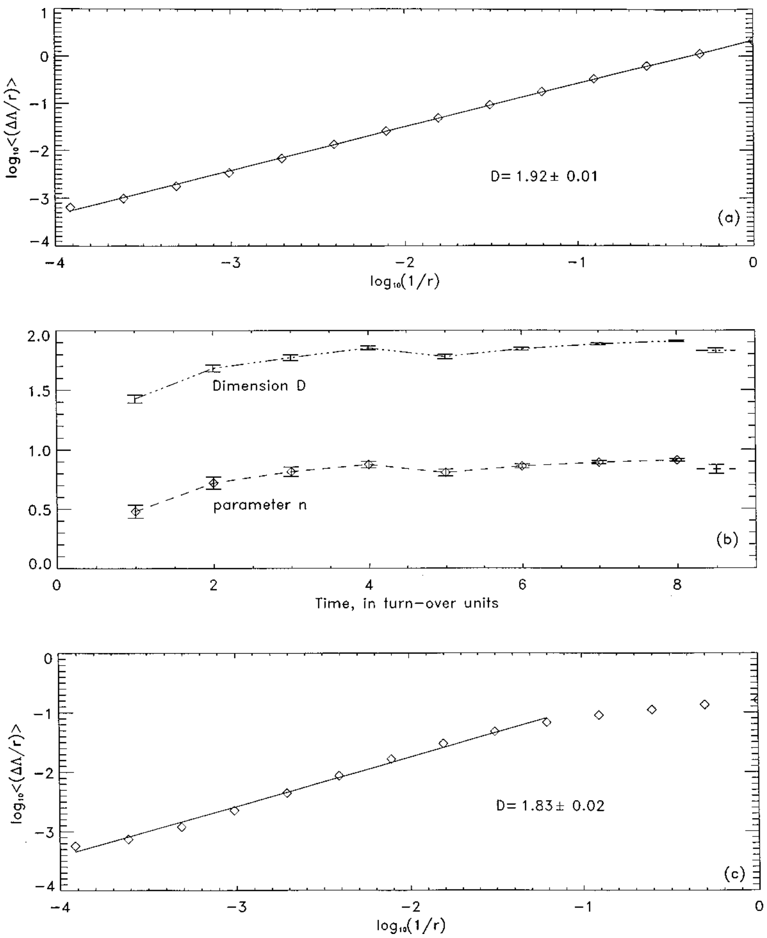

FIG. 10. Line scaling for the kinematic approach applied to the ABC flow, shown after 8 turnover times (a). Panel (b) shows the corresponding temporal evolution of the line fractal dimension D, and the evolution of the parameter n. As in Fig. 6, the latter parameter grows secularly. The corresponding nonlinear values for the parameter D (dashed–double-dotted line), together with its error bars, and for the parameter n (dashed line), together with its error bars, are also provided for comparison. It is important to note that these results are obtained after 16 turnover times, well outside the domain of this figure, and therefore their position along the abscissa is arbitrary. Panel (c) depicts the same result as (a), but for the nonlinear stage, after 16 turnover times.

The magnetic field line, naturally, becomes more smooth, due to nonlinear backreactions: the Lorentz force again smears out very small-scale irregularities. This results in a decrease of the scaling range [see Fig. 10(c)]. As the smearing acts on bigger scales, although less effectively, the scaling slopes become gentler, resulting in a decrease of both length dimension D and parameter n. This nonlinear smoothing, as usual, would decrease intermittency but, as already mentioned in Sec. V A, even in the kinematic approach the intermittency is negligible. As might be expected, the generalized dimensions calculated by Eq. (12) are practically trivial, i.e., ~ 1 (within the computational errors).

As mentioned in Sec. IV B, there are two competing effects, which may result in the nonlinear case in either increasing of singularity of the line, i.e., increasing of the length dimension D, and parameter n, or decreasing of singularity. These complications appeared, however, because the STF motion results in highly intermittent structures. As we saw, this is not the case for the ABC flow, and therefore the singularity of magnetic field lines only decreases, as seen from comparison of the dimension D given in Figs. 10(a) and 10(c). Both of these quantities, the dimension D and the parameter n for the nonlinear case after 16 turnover times, are shown in Fig. 10(b), in a comparison with the kinematic situation. One can see that, indeed, they decrease in the case of the nonlinear dynamo; this decrease is not substantial, however.

The intermittency fractal dimensions $D_q^{(i)}$, as defined by Eq. (16), are also trivial in the nonlinear case, as in the kinematic (see Sec. V A above).

As in the case of the STF flow, we can estimate the effective magnetic Reynolds number for the ABC flow directly from expression (1), using all the values obtained from reliable scaling. This calculation gives $R_m = 13\,865$.

We have also studied magnetic and velocity spectra. These runs have been made with as low a viscosity as was possible. As a result, the Reynolds number Re reached few million. As mentioned in Sec. II, this should not be misleading, however, because the motion and its random character are defined by random forcing (and not be instabilities, etc., typical for real turbulence). Recall that at the beginning, the magnetic field is large scale (i.e., it is a loop with radius $R = 3.5$), and the velocity field is given by the ABC flow with $k = 10$. We can see from Fig. 11(a) that shortly after the beginning, velocity pulsations are created, but the magnetic field is still large scale. After only one turnover time [cf. Figs. 11(b) and 11(c)], the magnetic field reaches equipartition. There is no real evolution of spectra after that, so that the spectra depicted in Fig. 11(d) present an average over times from 7.5 to 45.9 turnover times. The spectra show an equipartition of magnetic and kinetic energies, suggesting the presence of Alfvén waves with very large amplitudes. In fact, the large-scale field B_0 is weak, which means that the relative amplitude $\langle B^2 \rangle^{1/2}/B_0$ is very large: in the present simulations, this number is a few thousand in value. In spite of the large Reynolds numbers Re and R_m, it is hard to find an ''inertial range.'' Indeed, the spectra consist of two parts: the first, for $k \geqslant 250$, is rather steep, $\sim k^{-4}$, and definitely does not correspond to the inertial range; the second, for $20 \leqslant k \leqslant 250$, is more gentle, and therefore may be of more

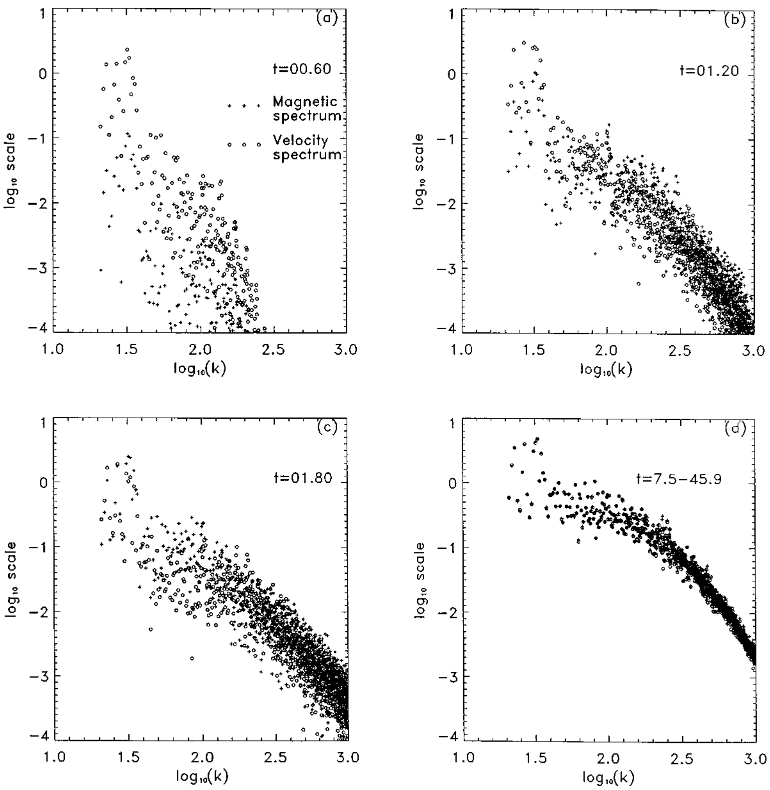

FIG. 11. Evolution of the magnetic and kinetic spectra. Panels (a)–(c) correspond to specific moments of time, as noted in the panels. Panel (d) shows the time average of such spectra, the average taken over the period from $t=7.5$ to $t=45.9$, in units of the turnover time.

interest. However, the dispersion of data points is large, and that would make any comparisons with power laws unreliable (as discussed in Sec. II). We note that the dynamics of the motion simply reflects the random forcing, which overpowers nonlinear interactions. Therefore, the spectrum is formed only in part by interactions of Alfvén waves.

An example of a magnetic field line which is initially a circle with radius $R=1$, after 16 turnover times, is depicted in Fig. 12(a). The initial Mach number is $M_A=10^2$. If the initial radius is instead $R=3.5$, then the final shape (after the same time interval) is depicted in Fig. 12(b). For comparison, we also show the same lines, but in the kinematic limit: panel (c) corresponds to $R=1$, and panel (d) to $R=3.5$. The time corresponds only to 8 turnover times (recall that in the kinematic limit, the resolution is lost much sooner than in the dynamic case, and therefore we are not able to proceed to larger time intervals). Note that all the lines depicted in Fig. 12 seem to be unresolved, consisting of straight line seg-

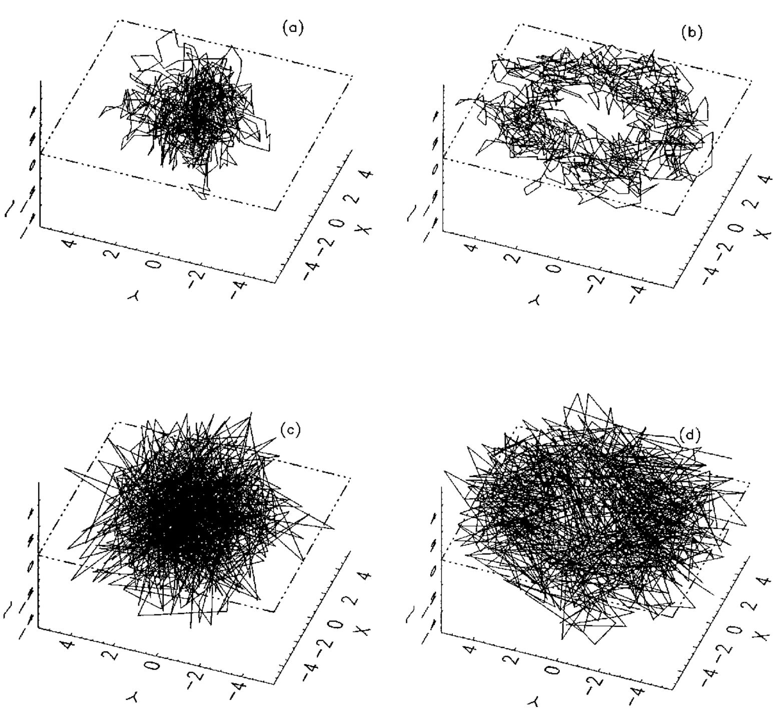

FIG. 12. Final image of a field line that started out at the beginning of a calculation as a circle with radius $R=1$ (a). Panel (b) corresponds to the same result but for an initial radius of $R=3.5$. Both panels depict the line after 16 turnover times of nonlinear evolution for the *ABC* flow. Panels (c) and (d) correspond to (a) and (b), but for the kinematic case, and only after 8 turnover times.

ments. This is, however, only in the image: the simulations are resolved, and we depicted only each fortieth point in the plot.

VI. TURBULENT DIFFUSION

In the kinematic approach, the behavior of a magnetic field line is analogous to that of any scalar field inserted into the turbulent flow. Thus, as one would expect, the length of the line grows exponentially, and becomes chaotic [as is indeed seen in Figs. 12(a) and 12(d)]. The line also ''diffuses'' in such a way that it occupies more than one dimension. In fact, the Kolmogorov capacity, that is, the box counting dimension, corresponds to the length dimension D (given in Figs. 3 and 10), and simply equals D [11]. Finally, the characteristic scale of the line, or its ''size,'' grows with time as $t^{1/2}$, as is typical for a random walk.

As a result, the matter is mixed at the same rate. In other words, a passive scalar field would also mix in a distance d, which grows with time as $\sim t^{1/2}$, i.e.,

$$d(t)=l\left(\frac{t}{\tau}\right)^{1/2}, \tag{18}$$

where τ is the correlation time (roughly, $\tau\sim l/v$). The distance d may be regarded as a radius of diffusion, with the property that all tracers would diffuse on this scale over a time interval t, and therefore any admixture would be mixed on this scale. If the tracer is also characterized by spatial structures larger than d, then these structures would be expected to be conserved on this time scale t, and any other structures whose spatial scales are smaller than, or comparable to, d would be mixed.

From another perspective, the displacement of a particle ξ also grows as $t^{1/2}$. One may say that the particle occupies a secularly increasing volume

$$V=d^3=l^3\left(\frac{t}{\tau}\right)^{3/2}, \tag{19}$$

or, in other words, there is a finite probability to find the particle in this growing volume. Therefore, the probability of finding the particle in a fixed volume ϵ is

$$\frac{\epsilon}{V}\sim\frac{1}{t^{3/2}}, \tag{20}$$

and the probability goes to zero as $t\rightarrow\infty$.

Finally, the distance between two infinitesimal close particles Δ grows exponentially,

$$\Delta=\Delta(t=0)e^{t/\tau}, \tag{21}$$

because of the positive Lyapunov exponent.

The situation is different if the initially weak magnetic field is allowed to react back on the fluid. The simulations show that a loop of radius $R=1$ expands, but only initially. When the magnetic field energy reaches equipartition, both the expansion and the diffusion stop. Indeed, the characteristic scale of the loop depicted in Fig. 12(a) is reached after a few turnover times, and then stays the same up to 16 turnover times, the figure corresponding to the last moment. The loop looks chaotic and dynamic, its shape is changing, but the size does not. This should be compared with that on Fig. 12(c), the size of the magnetic loop being bigger than that on panel (a), elapsed time being less (only 8 turnover times).

Panels (b) and (d) of Fig. 12 depict dynamics of magnetic loop with initial radius $R=3.5$. In the kinematic approach, the particles are diffusing in any direction, so that eventually all the volume V, Eq. (19), would be filled, panel (d). This happens when the radius of diffusion exceeds the initial size of the loop.

If the strength of the magnetic field is finite, then the radius of diffusion is restricted, and the loop still looks like a ring, or torus, panel (b). In order to estimate the radius of diffusion, note that the magnetic energy is growing,

$$\langle B^2\rangle=B(t=0)^2e^{2t/\tau}, \tag{22}$$

until it saturates in a fully developed nonlinear regime, at time $t=t_n$. At this moment of time, the diffusion radius has reached the value

$$d_n=l\left(\frac{t_n}{\tau}\right)^{1/2}.$$

Substituting the time t_n from Eq. (22) into this expression, we get for the nonlinear radius of diffusion,

$$d_n=l\left(\frac{1}{2}\ln\frac{\langle B^2\rangle}{B(t=0)^2}\right)^{1/2}. \tag{23}$$

Recalling that in our simulations the large-scale component of the field does not really change, we may write $\langle B_0^2\rangle$ instead of $B(t=0)^2$ in Eq. (23). Then, this rough estimation would give $d_n=2l$, and $l=\pi/10=0.31$. Thus, $d_n=0.63$. The characteristic thickness of the ring is thus $2d_n=1.26$, which is indeed the case, as seen from the Fig. 12(b). This size is comparable with initial size of the loop depicted on panel (a), and therefore, we do not see a ring, but rather filled volume of the size d_n+1 (the unity being the initial size of the loop).

The process of mixing can be seen from Figs. 13 and 14. Five magnetic field lines are painted in different colors [the line in the middle is painted in the same color as the background, and therefore cannot be noticed on Figs. 13(a) and 14(a)]. In the kinematic approach (Fig. 13), the lightest field line is mixed with the darkest, and after 16 turnover cycles everything is almost totally mixed up. In the nonlinear case (Fig. 14), the lines diffuse and spread, as in the kinematic approach, but only at the beginning. A light ''halo'' remains persistent, and dark field lines never mix with the light ones, although neighboring lines do mix. This happens because the distance between neighboring lines is less than, or comparable to, d_n, while the distance between the darkest and lightest lines is bigger. Thus, the radius of diffusion is restricted, and so is the diffusion itself.

In the kinematic approach, the probability of finding a particle in some fixed volume goes to zero according to Eq. (20). In nonlinear restricted diffusion, the particle remains inside a sphere of a radius d_n, centered at the initial position of the particle. To be more specific, it may walk out from the sphere, but with low probability: it stays inside the sphere most of the time. Therefore, two particles that are initially infinitesimal close to each other are contained in two inter-

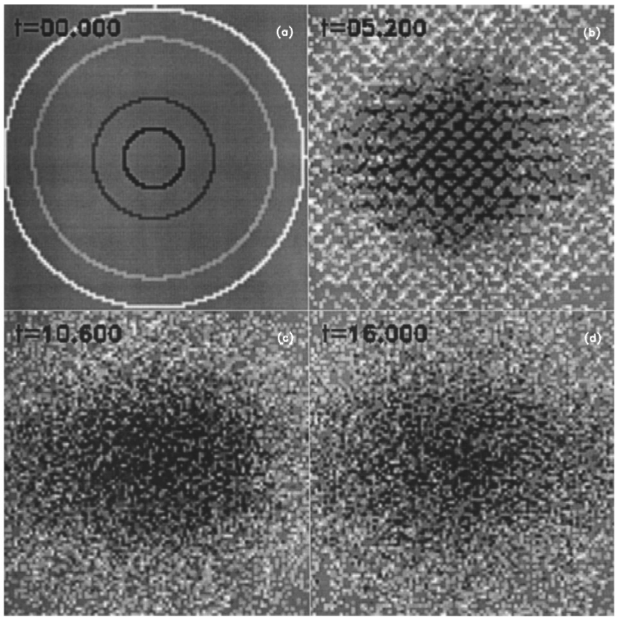

FIG. 13. Turbulent diffusion in the kinematic approach. The initial lines (a) are painted in various shades of gray, as indicated. After the turbulence is switched on, turbulent mixing takes place [see panels (b), (c), and (d)]. In the final stage, the lightest field line (which was initially on the periphery) penetrates to the very center, and the darkest field line (which was initially at the center, spreads out to the periphery. Thus, everything is well mixed.

secting spheres so that, in the long run, they do not separate farther than the diffusion radius. However, the process has a quasioscillating character, because after separating for a distance d_n, the particles would approach each other. In fact, this kind of turbulence is quite different from ''normal'' turbulence in a box of a size d_n. Due to the boundary conditions, the particles would not be able to travel distances bigger than d_n. However, in highly conductive media, the magnetic field would grow and, if the back reaction can be neglected, this growth would be unlimited. Now, if the initial strength of the magnetic field is weak but finite, then the magnetic field would grow only up to a point, and after that the magnetic energy is kept constant (in the statistical sense). Thus, in the ''regular'' case (with infinitesimal fields), the field grows, meaning that the distance between two infinitesimally close particles grows. In the nonlinear regime, the field does not grow, nor does the distance between particles.

Roughly speaking, the probability to find two particles in a volume Δ^3, that is, the distance between them is no more than Δ, is

$$\frac{\Delta^3}{d_n^3},$$

and, unlike expression (20), does not go to zero as $t \to \infty$. This means that the Lyapunov exponent is zero in the nonlinear regime. Note that suppression of Lyapunov exponents in nonlinear dynamos is well known (see, e.g., [3], Chap. 12, and references therein).

In spite of a vanishing Lyapunov exponent, the system is rather ''chaotic.'' First of all, the forcing is given as a random (in time) field. If we define a trajectory of the forcing, via the equation

$$\frac{d\boldsymbol{\xi}}{dt} = \mathbf{F},$$

then the Lyapunov exponent would be positive. Moreover, the exact position of the particle at specific moment of time inside the sphere of radius d_n, is unpredictable; all one really knows is the probability to find a particle within some volume. The particle has finite ''memory'' about its position, although it moreover ''memorizes'' its initial position, and so stays within the sphere.

The real displacement is defined by the equation

$$\frac{d\boldsymbol{\xi}}{dt} = \mathbf{v}(\mathbf{x},t) = \mathbf{v}_L(\mathbf{x}_0,t), \tag{24}$$

where $\mathbf{v}_L(\mathbf{x}_0,t)$ is the Lagrangian velocity of a particle starting at $\mathbf{x} = \mathbf{x}_0$. All the transport coefficients are defined through appropriate moments of the displacement. In particular, turbulent diffusion is defined by the relation

$$D_T = \frac{d}{dt}\langle \xi^2 \rangle. \tag{25}$$

In the kinematic approach, $\langle \xi^2 \rangle = l^2 t/\tau$, by Eq. (18), so that $D_T = l^2/\tau$. In the nonlinear regime, $\langle \xi^2 \rangle = d_n^2 = \text{const}$, and therefore $D_T = 0$.

The same situation holds with another transport coefficient, α, which is actually the generation coefficient of classical kinematic dynamo theory. According to [16],

$$\alpha = -\frac{d}{dt}\langle \boldsymbol{\xi} \cdot \boldsymbol{\nabla} \times \boldsymbol{\xi} \rangle,$$

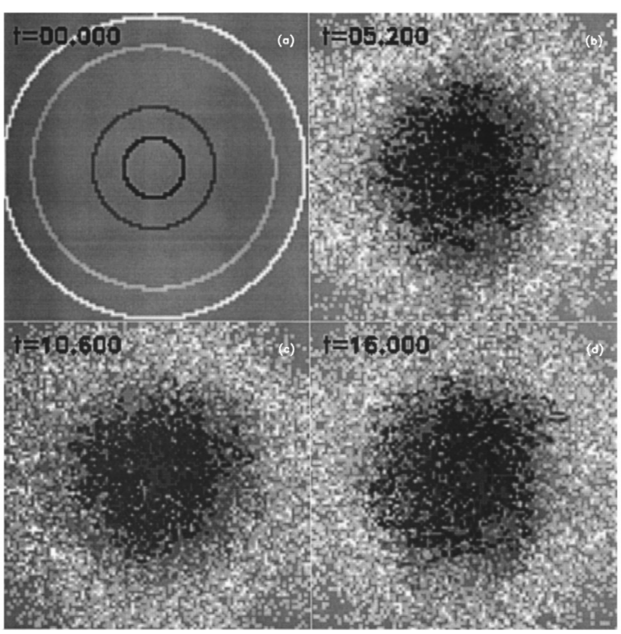

FIG. 14. Same as on Fig. 13, but in the nonlinear regime, that is, for an initial field with low but finite strength. It can be seen that the light ''stuff'' is never mixed with the dark ''stuff''; thus magnetic field mixing and decay is inhibited.

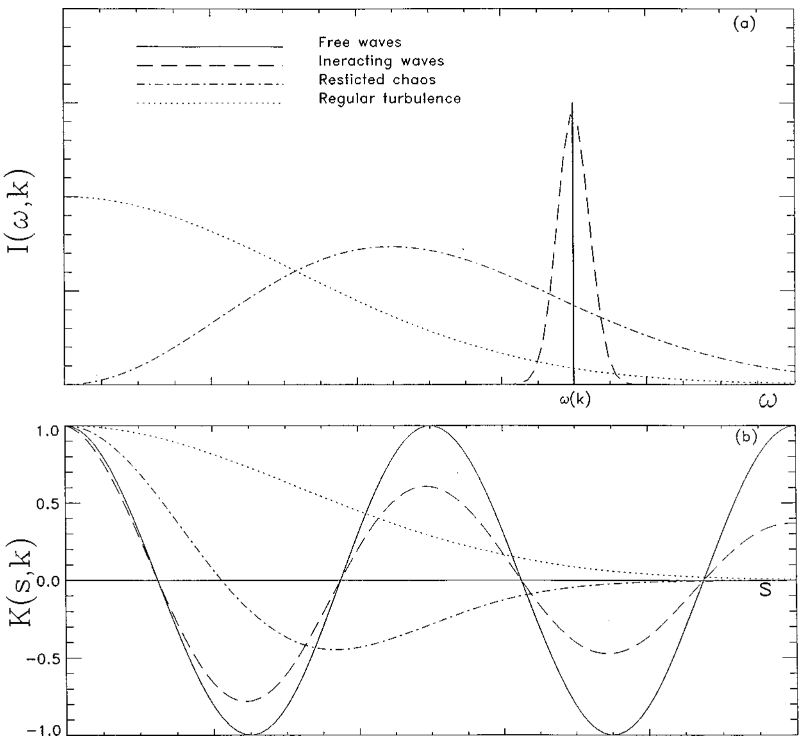

FIG. 15. Illustration of typical spectrum functions (a), and correlation functions (b) for a fixed wave vector k.

and, as $\boldsymbol{\xi}$ does not grow in the nonlinear regime, the generation coefficient $\alpha \to 0$ [8]. More generally, as mentioned in the Introduction, the generation is not possible without effective diffusion, and therefore, turbulent diffusion is vital to understanding magnetic dynamo.

The turbulent diffusion coefficient can be defined directly from the definition of the displacement (24). In order to do this, note that

$$\langle \xi^2 \rangle = 2\int_0^t (t-s) K(s) ds, \tag{26}$$

where

$$K(s) = \langle \mathbf{v}_L(\mathbf{x},t) \cdot \mathbf{v}_L(\mathbf{x},t+s) \rangle.$$

Obviously, asymptotically, as $t \to \infty$, the right-hand side of Eq. (26) behaves as $2t\int_0^\infty K(s)ds = t\int_{-\infty}^\infty K(s)ds$, so that, according to Eq. (25),

$$D_T = \int_{-\infty}^{\infty} K(s) ds. \tag{27}$$

In Fourier space,

$$\mathbf{v}_L(\mathbf{x},t) = \int \mathbf{v}(\mathbf{k},\omega) e^{i\omega t + i\mathbf{k}\cdot\mathbf{x}} d\omega \, d\mathbf{k},$$

and

$$\langle \mathbf{v}(\mathbf{k},\omega) \cdot \mathbf{v}(\mathbf{k}',\omega') \rangle = I(\omega,\mathbf{k}) \delta(\mathbf{k}+\mathbf{k}') \delta(\omega+\omega'),$$

where $I(\omega,\mathbf{k})$ is time-space spectrum. Now,

$$K(s,\mathbf{k}) = \int I(\omega,\mathbf{k}) e^{-i\omega s} d\omega,$$

and

$$K(s) = \int K(s,\mathbf{k}) d\omega \, d\mathbf{k},$$

so that, by Eq. (27),

$$D_T = \int I(0,\mathbf{k}) d\mathbf{k}. \tag{28}$$

Thus, the spectrum at zeroth frequency defines the diffusion coefficient [6]. As $I(0,\mathbf{k})$ is non-negative, the turbulent diffusion coefficient vanishes if and only if $I(0,\mathbf{k}) = 0$ for all wave vectors $\mathbf{k}$.

Figure 15 illustrates a few typical examples, for fixed wave vector $\mathbf{k}$. An ensemble of free waves corresponds to a delta function dependence, $I(\omega,\mathbf{k}) \sim \delta(\omega - \omega(\mathbf{k}))$, where $\omega(\mathbf{k})$ is dispersion relationship for these waves. The system has infinite memory, so that the correlation function, depicted in Fig. 15(b), ''never forgets'' its initial value (the function is simple a cosinusoid). If the waves interact, the process is referred to as weak turbulence, and the random phase approximation is valid. The delta function is broadened, and the memory time is large, but finite [cf. the corresponding correlation function in Fig. 15(b)]. An important feature of weak turbulence is that $I(0,\mathbf{k}) = 0$. Strongly interacting waves lead to a loss of their identities, that is, the dispersion relationship is no longer valid. Indeed, one should not call these features waves any longer. Nevertheless, if the equation $I(0,\mathbf{k}) = 0$ is still satisfied, then the process may be called ''restricted chaos.'' The corresponding correlation function possesses finite correlation time, but always contains an anticorrelation part [see Fig. 15(b)]. This corresponds to a return of all particles to their initial position. Thus, on the one hand, the process does have finite memory, because it ''forgets'' any specific position of the particle in diffusion radius; but on the other hand, it does remember forever the initial position of every particle, so that the diffusion sphere is centered at this point. Finally, regular turbulence results in the usual random walk, and $I(0,\mathbf{k})>0$.

It is noteworthy that restricted chaos is not a fundamentally new concept. Consider, for example, turbulence as commonly understood. The corresponding $I(\omega,\mathbf{k})$ spectrum for the velocity field $\mathbf{v}$ is depicted by a dotted line in Fig. 15(a); and we know that $I(0,\mathbf{k})>0$. However, the spectrum for the time derivative of the velocity, that is, for the acceleration field $\mathbf{a}=d\mathbf{v}/dt$, does vanish at the origin, because the spectrum for the $\mathbf{a}$ field is simply $I(\omega,\mathbf{k})\omega^2$, and this expression goes to zero at $\omega=0$. In spite of this fact, the acceleration field is of course a random field.

Restricted chaos is peculiar because the Lyapunov exponent vanishes. However, the exponent for this process is positive in phase specie: this is another way in which it resembles regular chaos. Indeed, suppose we consider two different realizations of the process, with the same forcing, but with different initial velocities. If the difference is infinitesimal small, then for a given initial position of a particle, the trajectories of these two processes would slightly differ only at the beginning. In spite of the fact that these two trajectories are kept within the same diffusive radius d_n, they eventually diverge, and become completely different. In that case, the final velocities of these two particles are different and uncorrelated as well.

Thus, weak initial fields may result in suppression of transport coefficients, that is, in restricted chaos. It is interesting to note that this statement is valid if the initial magnetic energy is much less than the kinetic energy, that is, in the content of a dynamo. In other words, the initial magnetic Mach number M_A should be big. In the opposite extreme, $M_A \ll 1$, an ensemble of Alfvén waves might result in the generation of convective cells, which are able to mix the matter [18]; in that case, an Alfvén wave decays into another Alfvén wave pulse convective cell with zero frequency. The spectrum $I(\omega,\mathbf{k})$ acquires a positive contribution at zeroth ω because of this zero frequency convection cell, and thus mixing becomes possible. The most important requirement for this process to occur is the geometry of field lines. That is, it should be possible to interchange magnetic field lines, and only then will the quasi-two-dimensional turbulence, i.e., these convective cells, appear. Obviously, this could happen if the field lines are simply straight lines, or if the field lines are circles. It now becomes clearer why the condition $M_A \ll 1$ should be satisfied. Indeed, in this case, the field lines are only slightly distorted by the motion, and these lines can be interchanged. If this condition is not satisfied, as in the case of a dynamo, then the magnetic field lines appear as depicted in Fig. 12: they are very complicated and are closely interwoven, so that their interchange becomes impossible. That explains why the diffusion is restricted by this weak field, as seen from Fig. 14.

VII. SUMMARY AND CONCLUSIONS

We have applied our Lagrangian approach to solving the magnetic dynamo equations [11] to two distinct nonlinear dynamo models, the STF dynamo and the *ABC* flow dynamo. This approach has the definite advantage that it allows us to work in the ideal MHD limit, so that the effective magnetic Reynolds numbers are very large (at least when compared to what can be accomplished by numerically solving the Eulerian equations).

Some of our results are not unexpected. Thus, the nonlinear STF results show saturation of the magnetic energy as the calculation proceeds, with the energy in the large-scale field component far below that associated with the small-scale magnetic fluctuations. In contrast, it was somewhat surprising that the exponent n in the relation [7]

$$\frac{\langle B^2\rangle}{\langle B_0^2\rangle}\sim R_m^n$$

is of order unity. This result suggests that magnetic field lines become less singular in the sense of intermittency, but also that they may become even ''longer'' as compared with line stretching in the kinematic regime. We now understand why this is so: the nonlinear effects first suppress the very small-scale line deformation.

We also studied random *ABC* flows in the kinematic regime, with the result that (again) the magnetic energy grows exponentially, but without any evidence for significant growth of the large-scale field component. When we extended this study to the nonlinear regime, we also find (as in the STF case) that the magnetic energy saturates at levels near equipartition with the kinetic energy. Furthermore, we find that the magnetic energy is mostly concentrated on (small) diffusive scales. While we observe ''regular'' diffusion in the linear regime, we see instead strong suppression of diffusion in the nonlinear regime. This suppression has the interesting feature that the field is mixed only on intermediate scales (of order of l, the size of the cells); because the spatial scale of the large-scale field is much larger than this scale (by definition), it cannot be mixed. We refer to this behavior as ''restricted chaos,'' in which the normal Lyapunov exponent (defined in configuration space) vanishes, but the Lyapunov exponent defined for paths in the phase space is positive.

ACKNOWLEDGMENTS

We gratefully acknowledge discussions with S. Childress, E. Ott, V. Zacharov, F. Cattaneo, E.-J. Kim, E. N. Parker, P. Diamond, C. Lindsey, E. Levy, and R. Jokipii.

APPENDIX

In this appendix, we discuss the forcing necessary to achieve an STF-like flow. Not surprisingly, this forcing is quite similar to the STF velocity field itself. We focus below on the specific can described by dynamic equation (4) in order to illustrate the general procedure. The first step, ''stretch,'' is described by

$$\hat{S}:\quad \mathbf{F}_1=a_1 e^{-\mathbf{x}^2/R_1^2}\{x-2xz^2/R_1^2,y-2yz^2/R_1^2,-2z +2(x^2+y^2)z/R_1^2\}.$$

The corresponding velocity stretches all field lines not far from the $z=0$ plane, and (because of the assumed damping exponent, or requirement that the motion is bounded) leads to the opposite process on the periphery, namely, compression of field lines. Therefore, we have to restrict ourselves to regions not far from $z=0$.

Next, we make a figure ''eight'' from the loop, compressing it along the y axis,

$$\hat{T}_1: \quad \mathbf{F}_2=a_2 e^{-x^2/R_2^2-(y^2+z^2)/r_2^2} \times\{0,-+2yz^2/r_2^2,z-2zy^2/r_2^2\}.$$

The next step is to twist about the x axis, described by

$$\hat{T}_2: \quad \mathbf{F}_3=a_3 e^{-\mathbf{x}^2/R_3^2}\{0,\omega(x)z-xz(y^2+z^2)/R_3^2, -\omega(x)y+xy(y^2+z^2)/R_3^2\},\omega(x)=x.$$

Now the loop should lie in the XZ plane, and we want to fold it in the y direction. This can be accomplished by the motion

$$\hat{F}: \quad \mathbf{F}_4=a_4 e^{-y^2/R_4^2-(x^2+z^2)/r_4^2}\{-x+2(xy^2+cx^3y)/R_4^2,y +3cx^2-2(x^2y+cx^4)/r_4^2,0\}.$$

We end up with a loop in the y-z plane, centered at some positive value of y (and $x=z=0$). We have to shift it back, so that the center is at $y=0$, and turn it about the y axis.

As a final aside regarding this STF flow, we note that there are 12 distinct parameters which define this flow: a_1, a_2, a_3, a_4, r_2, r_4, R_1, R_2, R_3, R_4, c, and τ. In our simulations, $a_1=1.8$, $a_2=3.0$, $a_3=6.6$, $a_4=1.0$, $R_1=0.7$, $R_2=0.3$, $r_2=1.0$, $R_3=0.71$, $R_4=1.5$, $r_4=0.7$, $c=1.9$, and $\tau=0.1$.

[1] Ya. B. Zel'dovich, Zh. Éksp. Teor. Fiz. **31**, 154 (1956) [Sov. Phys. JETP **4**, 460 (1957)].

[2] T. G. Cowling, Mon. Not. R. Astron. Soc. **140**, 39 (1934).

[3] S. Childress and A. D. Gilbert, *Stretch, Twist and Fold: Fast Dynamo* (Springer-Verlag, Berlin, 1995).

[4] See, e.g., B. J. Bayly, Phys. Rev. Lett. **57**, 2800 (1986); A. D. Gilbert and S. Childress, *ibid.* **65**, 2133 (1990).

[5] H. K. Moffatt and M. R. E. Proctor, J. Fluid Mech. **154**, 493 (1985).

[6] S. I. Vainshtein and Ya. B. Zel'dovich, Usp. Fiz. Nauk. **106**, 431 (1972) [Sov. Phys. Usp. **15**, 159 (1972)].

[7] S. I. Vainshtein and R. Rosner, Astrophys. J. **376**, 199 (1991).

[8] S. I. Vainshtein and F. Cattaneo, Astrophys. J. **393**, 165 (1992).

[9] E. N. Parker, *Cosmical Magnetic Fields* (Clarendon Press, Oxford, 1979).

[10] L. D. Landau and E. M. Lifshitz, *Electrodynamics of Continuous Media* (Pergamon, New York, 1984), Sec. 74.

[11] S. I. Vainshtein, R. Z. Sagdeev, R. Rosner, and E.-J. Kim, Phys. Rev. E **53**, 4729 (1996).

[12] F. Cattaneo and S. I. Vainshtein, Astrophys. J. **376**, L21 (1991); R. M. Kulsrud and S. W. Anderson, *ibid.* **396**, 606 (1992); L. Tao, F. Cattaneo, and S. I. Vainshtein, in *Solar and Planetary Dynamos*, edited by M. R. E. Proctor, P. C. Matthews, and A. M. Rucklidge (Cambridge University Press, Cambridge, 1993); S. I. Vainshtein, L. Tao, F. Cattaneo, and R. Rosner, *ibid.*; C. A. Jones and D. J. Galloway, *ibid.*; A. V. Gruzinov and P. H. Diamond, Phys. Rev. Lett. **72**, 1651 (1994).

[13] F. Cattaneo and D. W. Hughes, Phys. Rev. E **54**, 4532 (1996).

[14] S. I. Vainshtein, K. R. Sreenivasan, R. T. Pierrehumbert, V. Kashyap, and A. Juneja, Phys. Rev. E **50**, 1823 (1994).

[15] E. Ott, S. I. Vainshtein, in *Research Trends in Physics: Plasma Astrophysics*, La Jolla International School for Physics Studies, edited by R. Kulsrud, G. Burbidge, and V. Stefan (American Institute of Physics, New York, 1996). As this reference is not readily available, we give a brief derivation of this formula. We use a formula for the exponents for structure functions (2.9) from [14], which leads to the result for the vector potential **A** of the magnetic field **A**: $S_2(r)=\langle[\mathbf{A}(\mathbf{x}+\mathbf{r})-\mathbf{A}(\mathbf{x})]^2\rangle\sim\langle B_0^2\rangle l^2(r/l)^{\xi_2}$, $\xi_2=(1-\kappa)2-(1-D_2)$. Putting $r=\delta$, and noticing that $A/\delta\sim B$, that is, $\langle B^2\rangle\sim S_2(\delta)/\delta^2$, we have $\langle B^2\rangle/\langle B_0^2\rangle\sim(\delta/l)^{\xi_2-2=-2\kappa-(1-D_2)}$. Using definition (9) for the Reynolds number, we recover (1), with n obeying Eq. (15).

[16] H. K. Moffatt, *Magnetic Field Generation in Electrically Conducting Fluids* (Cambridge University Press, Cambridge, 1978).

[17] S. I. Vainshtein, A. M. Bykov, and I. N. Toptygin, *Turbulence, Current Sheets, and Shocks and Cosmic Plasma* (Gordon & Breach, New York, 1993).

[18] R. Z. Sagdeev, V. D. Shapiro, and V. I. Shevchenko, Pis'ma Zh. Éksp. Teor. Fiz. **27**, 361 (1978) [JETP Lett. **27**, 340 (1978)].